IIETA International Information and Engineering Technology Association
Advancing the World of Information and Engineering

Traitement du Signal
Vol. 42, No. 1, February, 2025, pp. 343-352
Journal homepage: http://iieta.org/journals/ts

An Accurate Diagnosis and Classification of Breast Mammogram Using Transfer Learning in Deep Convolutional Neural Network

Thiyagarajan Annamalai[1*], Murukesh Chinnasamy[2], Mary Joans Samuel Soundara Pandian[2]

[1] Department of Information Technology, Sri Venkateswara College of Engineering, Kanchipuram 602117, India
[2] Department of Electronics and Communication Engineering, Velammal Engineering College, Chennai 600066, India

Corresponding Author Email: thiyagarajana@svce.ac.in

https://doi.org/10.18280/ts.420129

Received: 9 July 2024
Revised: 27 September 2024
Accepted: 6 November 2024
Available online: 28 February 2025

Keywords:
breast cancer, mammogram, deep learning, transfer learning, modified Inception v3, classification.

ABSTRACT

Timely and precise identification of breast cancer (BC) is essential for enhancing patient results. This work investigates the capacity of deep learning to automate the categorization of BC using mammogram images. Our proposal involves using transfer learning with a customized Inception v3 architecture. This method utilizes pre-trained characteristics to tailor the model to the particular mammogram domain. Next, modified the last layers of the network and refined it using a mammogram dataset for classification. We assess the efficacy of our adapted Inception v3 model on a standard mammogram dataset, contrasting it with other deep learning structures and conventional machine learning techniques. The suggested technique demonstrates higher accuracy, sensitivity, and specificity in distinguishing normal and malignant breast tissue when compared to other approaches. This modified Inception v3 architecture has the capacity to strengthen the effectiveness in addition to the precision of breast cancer screening, eventually resulting in improved patient care. The proposed work is evaluated in comparison to other existing methodologies, including Inception v3, Inception v2, and VGG 16 and 19. The proposed modified Inception v3 model achieves 96.1% which is comparatively higher than the other methods.

1. INTRODUCTION

Utilizing computer-aided detection (CAD) technologies for early mammogram detection may enhance treatment results and increase survival rates for breast cancer patients. Conventional CAD software depends on manually identified features, which have limitations. Hand-crafted features are sometimes peculiar to a particular field and the process of designing them may be laborious, challenging, and not easily transferable.

CAD methods enhance early breast cancer identification and treatment results; nevertheless, conventional CAD depends on human-designed features that are frequently arduous, domain-specific, and challenging to transfer between datasets. Progress in deep learning, specifically the Convolutional Neural Networks (CNNs), provides a more effective method for the automatic extraction of information from medical images.

The development of a cancer tumor is attributed to the unregulated growth and division of cells, which subsequently invade and spread into the surrounding tissues within the human body [1]. The Convolutional Neural Network (CNN) is applied as another approach for extraction of features from the image directly [2]. CNN has excelled in several picture classification challenges. CNN has been used in medical picture categorization using the three primary methods. 1) Training a CNN from the beginning 2) Use of feature extraction 3) Adjusting a pre-trained model on images [3].

One effective transfer learning approach involves pre-training network parameters on source data, applying these parameters to the target domain, and then fine-tuning the network for improved performance. A methodology for locating and organizing multi-class breast cancer based on transfer learning has been suggested and put into practice in this scenario. The suggested model has two primary components [4]. The first component has six primary phases intended to improve the level of quality of the breast images. And second component is a hybrid deep learning algorithm that includes pre-trained CNN like VGG16 is used to transmit its acquired features to the mammogram classification [5].

Nonetheless, deficiencies persist in the diagnosis of multi-class breast cancer, especially with transfer learning. This research introduces an innovative methodology that improves image quality and utilizes a pre-trained CNN Modified Inception v3 for enhanced multi-class breast cancer classification.

2. RELATED WORK

Ting et al. [6] introduced a deep Convolutional Neural Network (CNN) with 28 unseen layers to classify breast cancer lesions. The model achieved 89% sensitivity, 91% accuracy, and 911% specificity by using feature-wise data augmentation. Togacar et al. [7] created BreastNet, a sophisticated architecture including convolutional, pooling, dense blocks

and residual which achieved a superior accuracy of 98.80% compared to AlexNet, VGG-16, and VGG-19 models.

Abbas [8] which contains a few steps for acquiring characteristics, transforming them into deep features, and training the features to make the ultimate selection. The model underwent testing using the MIAS dataset, resulting in a sensitivity of 92.1%, accuracy of 93.5%, specificity of 84.2%, and an AUC of 0.94. The findings indicate the design serves as an efficient tool for breast cancer categorization.

In their approach, Sha et al. [9] integrated two deep learning methods: CNNs, which are successful in image processing tasks, and the Grasshopper Optimization Algorithm, which is inspired by optimization methods found in nature. They showed remarkable performance with sensitivity, specificity, and accuracy rates of 97.5%, 94.3%, and 96.1%, respectively.

Lotter et al. [10] developed a model tailored for multi-class breast cancer categorization. ResNet50 is a generally utilized deep learning model renowned for its efficacy in image recognition. The system demonstrated remarkable performance with a sensitivity of 95.6%, showing its capability to reliably identify genuine positive instances. The specificity was reported as 95.8%, indicating its ability to accurately detect genuine negatives and reduce false positives. The AUC value of 0.93 indicates good discriminative power and overall efficacy in classification.

Cao et al. [11] achieved notable progress in TL for BC by not fine-tuning the source network layers. They focused on using ResNet-125, a deep neural network architecture, without modifying or fine-tuning its layers. Their technique was assessed using the "ICIAR 2018" dataset, a widely used benchmark dataset for testing medical images. Cao et al. [11] significantly improved an accuracy rate of 83.79% with their methods.

Deniz et al. [12] made modifications to the last few layers, and the assessment was performed on the BreaKHis dataset, which is widely utilized for diagnosing breast cancer. The model they created had an accuracy rate of about 91.37%. The fine-tuning strategy improved the AlexNet and VGG16 models' classification performance.

Celik et al. [13] used the DenseNet-161 model to implement a pre-training approach to improve classification accuracy. The author used the pre-trained DenseNet-161 model, which was previously trained on a huge dataset, and optimized it for the particular objective of classifying breast tumors using the BreaKHis dataset. They obtained an F-score of 92.38% and an accuracy of 91.57% with their excellent efforts. Table 1 illustrates the comparison of existing work. This study aims to automatically extract the afflicted patch by segmentation, decrease training time, and enhance the performance of classification.

Table 1. Comparison of existing work

Author	Methodology	Advantages	Disadvantages
Ting et al. [6]	Implemented a deep convolutional neural network of 28 novel layers, employing feature-wise data augmentation for breast cancer classification.	High sensitivity (89%), accuracy (91%), and specificity (91.1%) are attributed to deep learning networks and data augmentation.	Overfitting and higher computing expenses are possible outcomes of the 28-layer CNN's complexity.
Togacar et al. [7]	BreastNet, a complex architecture that outperformed VGG-16, VGG-19, and AlexNet thanks to its convolutional, pooling, dense block, and residual components.	Enhanced precision (98.80%) and increased efficiency via architectural design.	Increased computational complexity resulting from several blocks and residual components.
Abbas et al. [8]	Employed methodologies for feature capture, conversion into deep features, and classification, evaluated on the MIAS dataset.	Highly accurate categorization technique with an efficiency of 93.5%, sensitivity of 92.1%, and specificity of 84.2%.	Reduced specificity relative to other models, signifying an elevated false positive rate.
Sha et al. [9]	Integration of Convolutional Neural Networks (CNNs) with the Grasshopper Optimization Algorithm (GOA) for breast cancer diagnosis.	Exceptional sensitivity (97.5%), specificity (94.3%), and accuracy (96.1%) are attributable to nature-inspired optimization.	Integrating GOA with CNN may augment the model's complexity and prolong the training duration.
Lotter et al. [10]	Created a ResNet50-based model to categorize breast cancer into multiple classes and assessed its performance on multi-class datasets.	High sensitivity (95.6%), specificity (95.8%), and an AUC of 0.93 indicate excellent discriminative capability.	ResNet50 may necessitate fine-tuning and substantial datasets for optimal efficacy.
Cao et al. [11]	Employed ResNet-125 without fine-tuning the source network layers, evaluated on the ICIAR 2018 dataset.	Achieved moderate accuracy (83.79%) without any modifications or fine-tuning of the model.	Low accuracy relative to models that incorporate fine-tuning, demonstrating reduced flexibility to breast cancer pictures.
Deniz et al. [12]	Optimized AlexNet and VGG16 models, evaluated on the BreaKHis dataset for breast cancer diagnosis.	Fine-tuning enhanced classification, attaining 91.37% accuracy.	The fine-tuning methodology may necessitate substantial data and computational resources.
Celik et al. [13]	Employed DenseNet-161 with pre-training and fine-tuning on the BreaKHis dataset to enhance classification accuracy.	Attained a high F-score of 92.38% and an accuracy of 91.57% utilizing a robust pre-trained model.	DenseNet-161 necessitates substantial computational resources and data for optimal efficacy.

3. PROPOSED WORK

The approach for detecting and classifying breast cancer has two primary components. The first component is for preprocessing the picture, while the subsequent one is employed for transferring the CNN parameters [14]. Figure 1 displays the intricate structure of the proposed work.

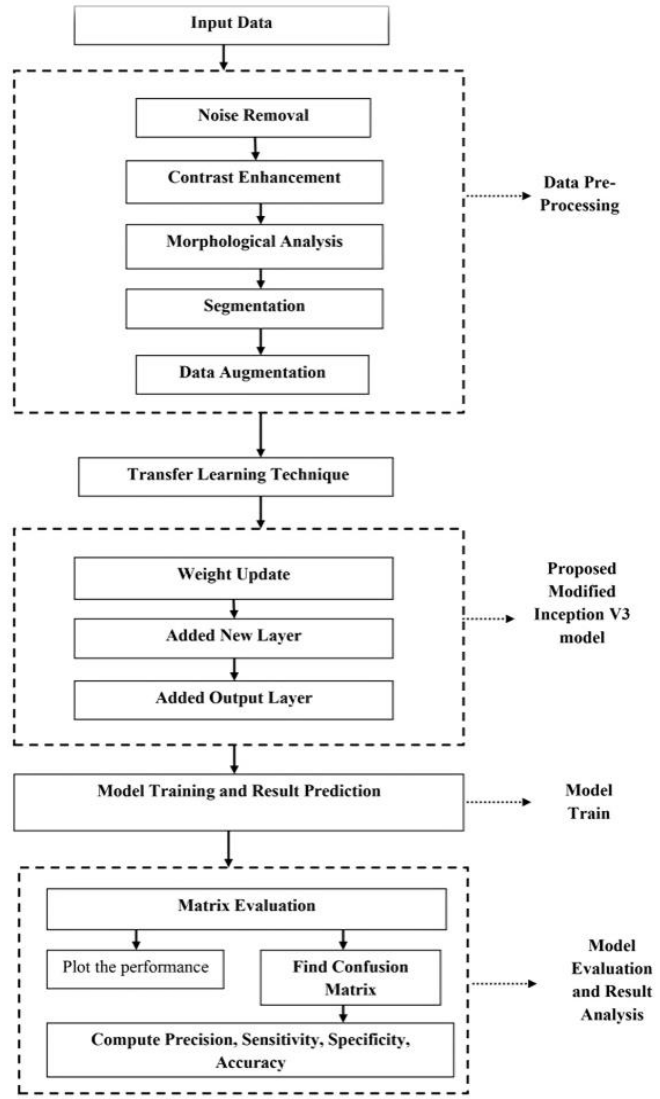

Figure 1. Proposed workflow

3.1 Image preprocessing

Image preprocessing is crucial in mammogram detection to improve image quality and ready it for precise analysis by CAD systems. Here are some essential stages.

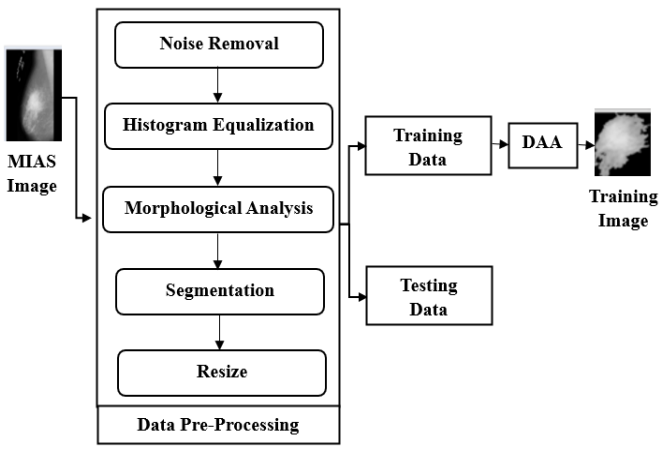

Figure 2. Levels of data preprocessing

Before the learning process is initiated, segmentation methods can be used to clearly auto detect the tumor areas. To cut down computing time, this is done. The enhancement of image visibility and the improvement of segmentation accuracy can be achieved by reducing background noise, equalization of histograms, and morphological analysis techniques prior to segmentation. Figure 2 illustrates that data preparation involves seven steps.

3.1.1 Noise removal

Mammograms can be affected by variety of noises, such as gaussian, speckle, salt-and-pepper noise. This noise may diminish the efficacy of classification methods. Using a 2D median filter may efficiently eliminate noise while retaining crucial information for categorization. Figure 3 displays the picture after the implementation of a 2D median filter.

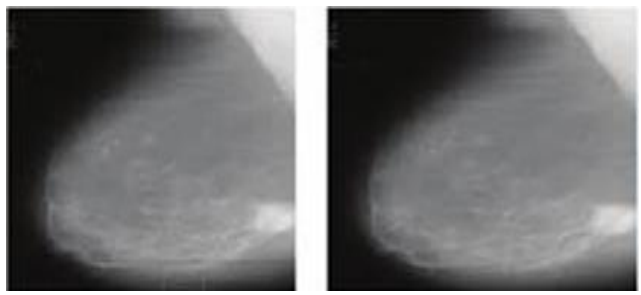

Figure 3. Normal vs noise removed image

Let $I_{med(x,y)}$ represent the intensity of the same pixel after applying a 2D median filter. The 2D median filter analyzes a square or rectangular neighborhood positioned in the middle of each pixel. Define $N_{x,y}$ as the *nXn* neighborhood centered at pixel (x,y). The median value, denoted as $I_{med(x,y)}$, is calculated as the median of pixel intensities in the neighborhood N_{xy}. Mathematically, the computation of $I_{med(x,y)}$ can be represented in Eq. (1) as follows:

$$I_{med(x,y)} = median(N_{xy}) \quad (1)$$

Algorithm 1: 2D median filter for noise removal

1) **Input:** load the mammogram image as a grayscale image $I_{(x,y)}$

2) **Define Kernel Size:** Determine the size of the square or rectangular neighborhood (kernel) around each pixel. Common choices include 3×3, 5×5, or 7×7 kernels, but the size can vary depending on the specific application and desired filtering effect.

3) **Initialize Output Image:** Generate a blank output image matrix with dimensions identical to the input picture to store the filtered image.

4) **Iteration:** Perform an iteration over every pixel's intensity (x, y) in the input image.

5) **Apply Median Filter:**

i. For each pixel location (x, y), define a neighborhood N_{xy} centered at that pixel, with a size determined by the kernel size.

ii. Collect the intensity of pixels in the surrounding area $N_{xy.}$

iii. Sort the intensity of pixels in ascending order.

iv. Determine the sorted pixel's median value. If the neighborhood's pixel count is even, take the average of the two intermediate values.

v. The computed median value is assigned to the equivalent pixel location in the output image.

6) **Output:** The resulting output image is the filtered image obtained after applying the 2D median filter to the input mammogram image.

3.1.2 Contrast enhancement

Histogram equalization (HE) is a prevalent method for improving picture contrast, often used in image processing, including mammograms. It adjusts the intensity levels of the picture to cover the whole dynamic range, improving contrast and making the image more visually attractive and simpler to analyze [15]. Figure 4 displays the original picture beside the image with contrast enhancement achieved using histogram equalization.

Figure 4. Contrast enhancement using HE

Algorithm 2: Histogram equalization for Contrast Enhancement

Input: The variable $I(x, y)$ represents a grayscale mammogram image. The pixel values in this image range from 0 to L-1. The variable L represents the number of intensity levels, which is typically set to 256 bits.

Output: $g(x, y)$-Contrast-enhanced mammogram image

1) **Calculate Histogram H(k):** Histogram of image I, where, H(k) represents the number of pixels with intensity k ($0 \leq k \leq L-1$)

2) **Normalize Histogram n(k):** The normalized histogram represented in Eq. (2), obtained by dividing $H(k)$ by the overall pixel ($M \times N$): Where M and N are the image height and width.

$$n(k) = \frac{H(k)}{M \times N} \tag{2}$$

3) **Calculate Cumulative Distribution Function (CDF):** $p(k)$: CDF of the normalized histogram, representing the probability of finding a pixel with intensity less than or equal to k, shown in Eq. (3):

$$p(k) = \sum_{i}^{k} n(i) \tag{3}$$

4) Map Intensities To New Values: $g(x, y)$ equalized image with enhanced contrast, represented in Eq. (4):

$$g(x, y) = L - 1 * p(I(x, y)) \tag{4}$$

3.1.3 Morphological analysis

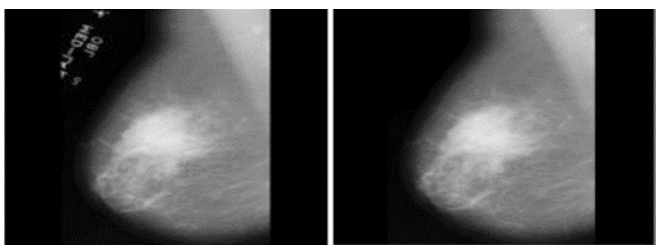

Figure 5. Original vs morphological mammogram image

Morphological analysis is a crucial step in eliminating non-breast areas prior to segmentation to ensure the accuracy of the findings. By applying the structural element (SE) to the input image, the necessary structures may be extracted during morphological operations. The resulting image obtained from this process retains the exact identical dimensions of the original input image displayed in Figure 5. The value of each pixel is based on the value of the pixel next to it and the value of the same pixel in the input picture.

Algorithm 3: Morphology Analysis

1) **Set Representation:** Every pixel in the mammogram is represented as a binary value (0 or 1), with 0 for black and 1 for white. The entire image is considered as a binary set X, where each element corresponds to a pixel.

2) **Structuring Element:** This is a small binary image defining the shape used for morphological operations. For instance, a 3×3 square with all ones represents a square SE. The size and shape of the SE significantly impact the outcome of operations.

3) **Erosion:** Erosion shrinks objects in the image by removing pixels that don't touch the SE when placed at every pixel location in X. Mathematically, erosion of set X by SE B (denoted as $X \ominus B$) is defined in Eq. (5), where B_X is the shifted version of B placed at pixel x.

$$X \ominus B = \{X \epsilon X | B_X \subseteq X\} \tag{5}$$

4) **Dilation:** Dilation expands objects by adding pixels that touch the SE when placed at every pixel location in X. Mathematically, dilation of set X by SE B (denoted as $X \oplus B$) is defined in Eq. (6):

$$X \oplus B = \{X | B_X \cap X \neq \emptyset\} \tag{6}$$

5) **Opening and Closing:** Opening combines erosion and dilation to remove small objects and smooth edges, represented in Eq. (7):

$$IO = Inp \ominus SE \oplus SE \tag{7}$$

Closing combines dilation and erosion to fill small holes and smooth edges, represented in Eq. (8):

$$IC = Inp \oplus SE \ominus SE \tag{8}$$

Opening and closing are defined using erosion and dilation iteratively.

3.2 Segmentation

By applying a threshold-based segmentation approach for automated region extraction, the calculation time may be minimized and the evaluation can be concentrated on the area most impacted by cancer. This work utilizes a global threshold for segmenting mammogram images.

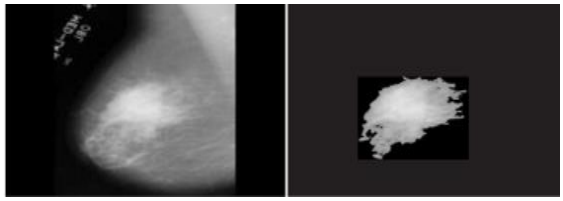

Figure 6. Original vs segmentation

Global thresholding is a common and straightforward technique used to segment images, such as mammograms. This approach involves applying a single threshold value to the whole picture to distinguish between foreground (breast tissue) and background. Figure 6 displays the segmented picture derived from the original.

Algorithm 4: Global Threshold based Segmentation

1) **Select Threshold Value T_h:** Which separates foreground and background in the grayscale image. This can be done manually or automatically using techniques like Otsu's method.

2) **Apply the threshold value T_h:** To the grayscale image. Here $M(x,y)$ shown in Eq. (9) is the binary mask indicating segmented regions.

$$M(x,y) = f(x) = \begin{cases} 1 \; if \; I(x,y) > T_h \\ 0 \; Otherwise \end{cases} \quad (9)$$

$I(x,y)$ is the intensity of the grayscale image at pixel (x,y). T_h is the threshold value. The resulting binary mask M(x,y) contains foreground regions (breast tissue) represented by pixel value 1, and background regions represented by pixel value.

3.3 Data augmentation

Deep learning techniques perform more well with extensive datasets. Data augmentation is an extensively used method to expand the dataset, which aids in mitigating overfitting when working with a tiny quantity of data during training. In this work, both training and testing data may be expanded by a series of changes.

The Data augmentation algorithm (DAA) is used to enhance the amount of input data. Figure 7 the segmented pictures undergo clockwise rotation by 90°, 180°, 270°, and 360°. Subsequently, each rotating picture is vertically mirrored. An input picture will generate eight images using this method.

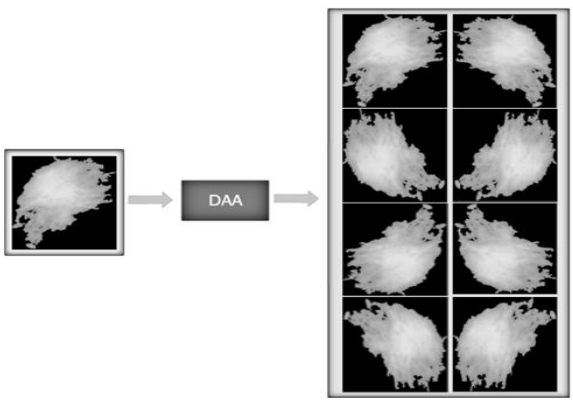

Figure 7. Image augmentation using DAA

Algorithm 5: Data Augmentation

1) Random Rotation: Rotate the image and corresponding label by a random angle within a specified range represented in Eqs. (10) and (11):

Image rotation

$$\text{Rotated Image} = \text{rotate}(\text{I}, \text{angle}) \quad (10)$$

Label Rotation

$$\text{Rotated Label} = \text{rotate}(\text{L}, \text{angle}) \quad (11)$$

2) Random Shear: Apply a random shear transformation to the image and label. Calculate the shear Transformation Matrix shown in Eq. (12):

$$\text{Shear Matrix} = \begin{bmatrix} 1 & \text{shear factor} \\ 0 & 1 \end{bmatrix} \quad (12)$$

Image Shear using Eq. (13):

$$\text{Sheared Image} = \text{affine transform}(\text{I}, \text{shear matrix}) \quad (13)$$

Label Shear using Eq. (14):

$$\text{Sheared label} = \text{affine transform}(\text{L}, \text{shear matrix}) \quad (14)$$

3) Random Zoom: Randomly zoom in or out of the image and label. Calculate zoomed shape using Eq. (15):

$$\text{Zoomed Shape} = (\text{int}(\text{h X zoom} - \text{facor}), \text{int}(\text{w X Zoom} - \text{factor})) \quad (15)$$

Image_Zoom using Eq. (16):

$$\text{Zoomed Image} = \text{zoom}(\text{I}, \text{zoom} - \text{factor}) \quad (16)$$

Label_Zoom using Eq. (17):

$$\text{Zoomed Label} = \text{zoom}(\text{L}, \text{zoom} - \text{factor}) \quad (17)$$

4) Random Horizontal flip: Represented in Eqs. (18) and (19). Optionally perform a horizontal flip with a probability of 0.5.

$$\text{Flipped Image} = \text{flip} - \text{left} - \text{right}(\text{I}) \quad (18)$$

$$\text{Flipped Label} = \text{flip} - \text{left} - \text{right}(\text{L}) \quad (19)$$

4. CLASSIFICATION

The suggested design employs transfer learning methodologies to describe models. The operation starts with a certain quantity of levels in the input layer, each exhibiting the enhanced pictures derived from the preceding step of data processing. The activation functions are not limited to the convolutional layers. This approach utilizes downsampling to identify certain features. By including a dropout layer, softmax layer, and fully connected layer, this process prevents overfitting. The result is calculated prior to using the categorization layer to predict the class [16].

4.1 Modified Inception v3

The deep feature maps are reduced in resolution using a downsampling technique with a stride factor of two. The essential Inception module is composed of three parallel routes that use 1×1, 3×3, and 5x5 convolution filters. The deep learning inception model addressed the issue of time utilization resulting from its extensive structure by applying down-sampling in addition to sparse associated layers within the convolutional layers. The dimensionality of feature maps was decreased by applying a 1×1 convolutional layer in each Inception module.

By implementing these techniques, the processing time

of models developed using deep learning may be reduced to match that of VGG-16 [17] or ResNet-50 [18]. A modified variant of the Inception deep learning networks, known as Modified InceptionV3, was created to fully use the benefits of using residual connections in deep learning models. Residual connections were used instead of filter concatenation in Inception models to enhance the training of deeper network structures, resulting in improved InceptionV3 deep learning models [19]. Training Inception models using residual connections is much faster, as shown by Cai et al. [20]. There is also an improvement in the residual Inception DL models' overall classification performance. The study enhanced InceptionV3 by substituting the last two layers with four levels of the Global Average Pooling (GAP) layer, two fully connected layers with Rectified Linear Unit (ReLU) activation functions, and a SoftMax logarithm layer. Figure 8 illustrates the modified Inception v3 model. Figure 9 illustrates the Inception v3 model architecture. The performance of classification can be improved by the classifier of the proposed CNN network.

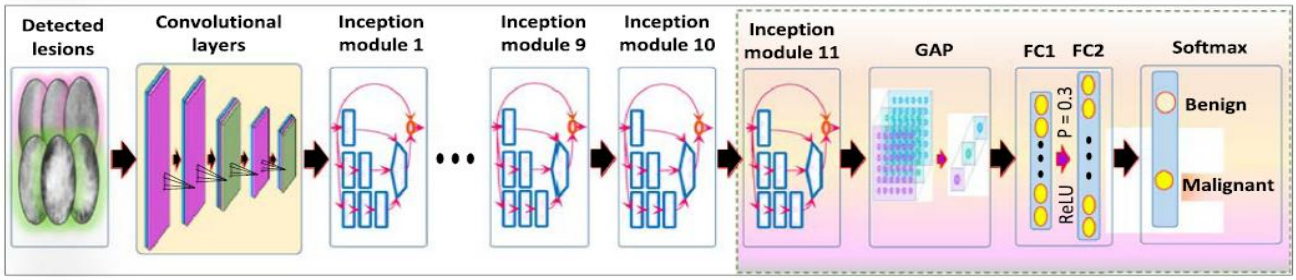

Figure 8. Modified Inception v3 layer architecture

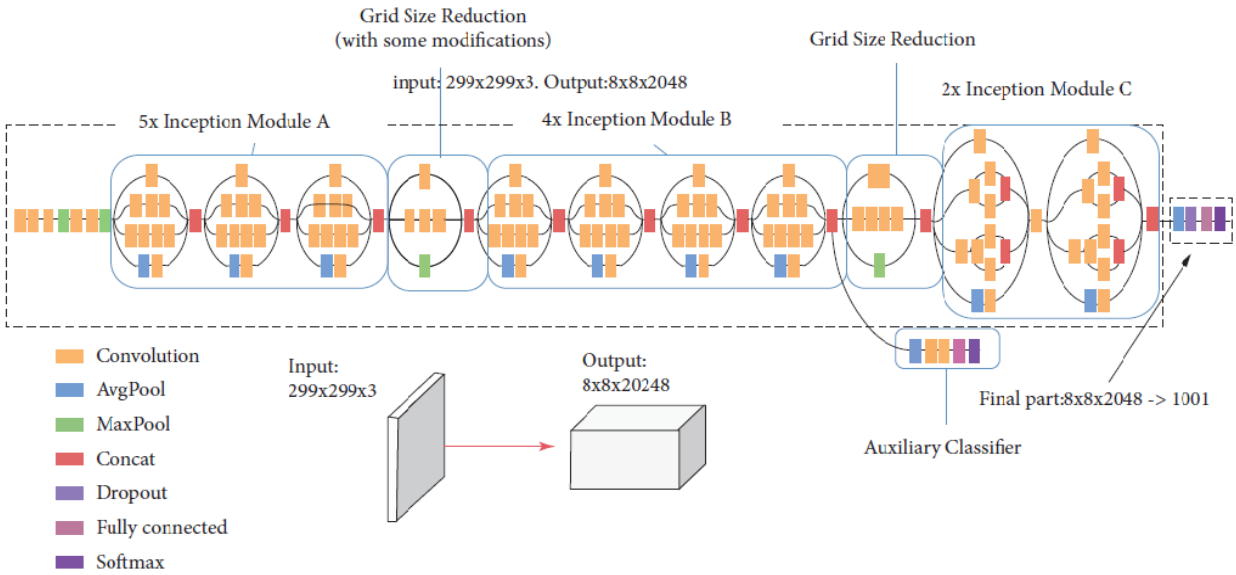

Figure 9. Inception v3 model architecture

4.2 Layers details of modified inception v3

The modified Inception v3 model applies the pre-trained Inception v3 model up to a designated layer, often before the final classification layers. This utilizes the model's capacity to extract universal picture characteristics. To ensure that the basic Inception v3 layers remain unchanged throughout training, it is necessary to freeze their weights, preventing any updates. This approach directs the learning process toward the changed components. Inception v3 has a strong dependence on convolutional layers. The layers use filters to process the incoming picture, extracting characteristics that vary in terms of size and orientation.

4.2.1 Global Average Pooling (GAP) layer

The GAP layer is used to reduce the spatial dimensions (height and width) of the feature maps to a singular value per feature map by means of averaging. This aids in diminishing the number of parameters and may serve as a preventive measure against overfitting. The GAP layer calculates the following using an input tensor $X \in A^{HXWXF}$ obtained from the output of the InceptionV3 base model, where height as H, width as W, and F is the number of channels (feature maps) shown in Eq. (20).

$$X_{GAP}[k] = \frac{1}{HXW}\sum_{i=1}^{H}\sum_{j=1}^{W} X[i,j,k] \quad \text{for k=1, 2, ……, F} \tag{20}$$

where,

$X_{GAP} \in R^F$ is the outcome of the GAP layer

$X[i,j,k]$ indicates the value of k^{th} feature map at the position (i,j)

4.2.2 Fully connected layer - dense layer

Following the GAP layer, the outcome is sent into a fully connected (Dense) layer to improve the features and decrease dimensionality. Let's represent the outcome of the GAP layer

as X_{GAP}. The Dense layer with ReLU activation is computed by Eq. (21).

$$X_{Dense1} = RELU(W_1.X_{GAP} + b_1) \quad (21)$$

where,

$W_1 \in R^{DXC}$ is the weight matrix

$b_1 \in R^D$ indicates the bias vector

D indicates the number of units in the Dense layer

ReLU(x)=max(0,x) is the ReLU activation function applied element-wise

$X_{Dense1} \in R^D$ is the output of the Dense layer

4.2.3 Dropout layer

A Dropout layer is incorporated after the Dense layer to mitigate the problem of overfitting is represented in Eq. (22):

$$X_{dropout} = Droupout(X_{dense1}, r) \quad (22)$$

where, r is the dropout rate

4.2.4 Output fully connected layer (Dense) with SoftMax function

Ultimately, the result obtained from the Dropout layer is sent onto a further Dense layer that utilizes SoftMax activation in Eq. (24) to provide probabilities for each class as shown in Eq. (23):

$$Y' = softmax(W_2.X_{Dropout} + b_2) \quad (23)$$

where,

$W_2 \in R^{KXD}$ is the weight matrix.

$b_1 \in R^k$ indicates the bias vector.

K indicates the number of output classes.

$$softmax(z_i) = \frac{e^{zi}}{\sum_{j=1}^{k} e^{zj}} \; for \; i = 1,2,\ldots..K \quad (24)$$

$y' \in R^k$ is the output probability vector.

The additional layers augment the retrieved characteristics from the InceptionV3 model and optimize them for the ultimate classification objective, rendering the model well-suited for mammogram classification.

5. EXPERIMENTAL SETUP

5.1 Dataset preparation

Table 2. Image details of the MIAS dataset before and after DAA

Type	Training	Testing	Training	Testing
	Original		After DAA	
Benign	48	13	2621	656
Malignant	41	11	2424	605
Normal	167	42	9022	2256

The proposed approach utilizes the well-known MIAS datasets to develop techniques for classifying breast cancer. The images within the MIAS collection are stored in portable gray map (PGM) format and possess dimensions of 1024×1024 pixels. The MIAS dataset comprises a total of 322 images that have been categorized into three distinct groups. Specifically, there are 61 images representing benign patients, 52 images representing malignant cases, and 209 images representing normal cases before DAA. The whole data is split randomly as 80-20 ratio for training and testing the details are shown in Table 2 and followed by the parameter setting in Table 3 [16, 21].

Table 3. Parameter setting

S.No.	Parameter	Value
1	Minimum size of batch	10
2	Maximum Epochs	20
3	Learn rate drop factor	0.5
4	Initial learn rate	1e-4
5	Learn rate drop period	5

5.2 Performance evaluation metrics

Various classifiers can be assessed with factors like accuracy, precision, recall, and F1-score. Sensitivity and specificity are measures of categorization accuracy, which are determined by true positive (TP), true negative (TN), false negative (FN), and false positive (FP) outcomes. The confusion matrix in Figure 10 is an essential method in deep learning for assessing the effectiveness of image classification.

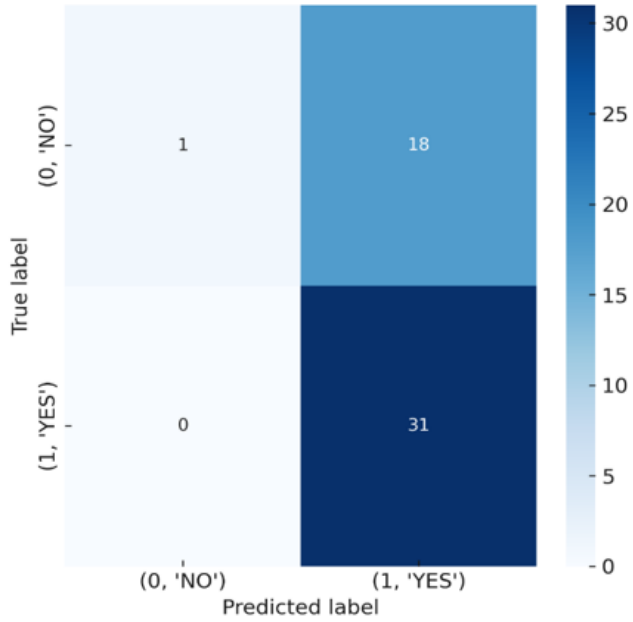

Figure 10. Confusion matrix

5.3 Confidence intervals

The formula used to determine the confidence interval based on a given metric is defined in Eq. (25).

$$CI = x' \pm Z \times \frac{\sigma}{\sqrt{n}} \quad (25)$$

The k-fold cross-validation with 10 folds is recorded then the mean accuracy of the model 0.8990 for a level of confidence of 95% and the critical value Z=1.96.

6. RESULT ANALYSIS

To scale and normalize all identified breast lesions, DAA interpolation is used. The resulting fixed sizes for CNN, ResNet-50, and Modified Inception v3 are 128×128, 224×224, and 299×299 pixels, respectively. One may adjust breast lesion photographs to various appropriate sizes.

Altered during the training of Inception-v3, the graph of training accuracy generally increases, but the graph of validation accuracy fluctuates. In Figure 11, both training and validation loss have been performed. In training loss, while considering accuracy there is no improvement from the start to 8 epochs. The validation accuracy experiences the most significant improvement after the 8th epoch, increasing from 0.82% in the 4th epoch to 0.86%. The validation loss curve displays erratic outcomes, but the training accuracy consistently improves until the last epoch, as seen in Figure 12.

Table 4. Performance of proposed Vs existing method

Classifier	ACC	SN	SP	PR	AUC	FS
Modified Inception v3	96.12	91.5	94.3	90.2	0.99	92.7
Inception v3	94.5	90.13	86.4	87.53	0.94	89.21
Inception V2	86.24	88.71	84.51	84.36	0.88	90
VGG 19	87.13	89.32	83.17	86.5	0.83	94
VGG 16	84.56	79.62	81.5	87.2	0.89	90
Resnet 50	89.2	83.13	79.3	80.2	0.79	91.23

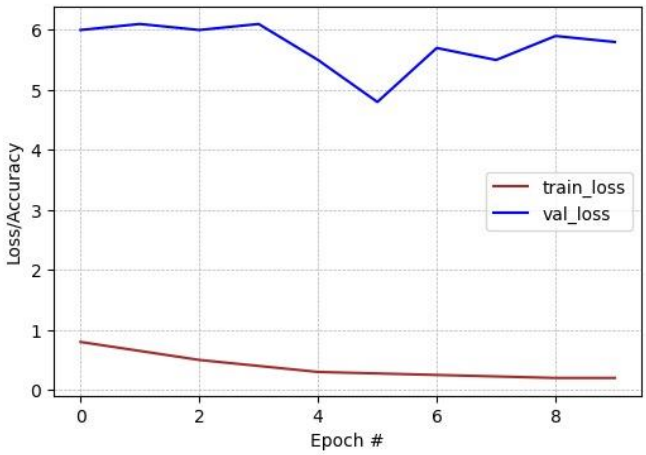

Figure 11. Training and validation curve of the modified Inception v3 classifier

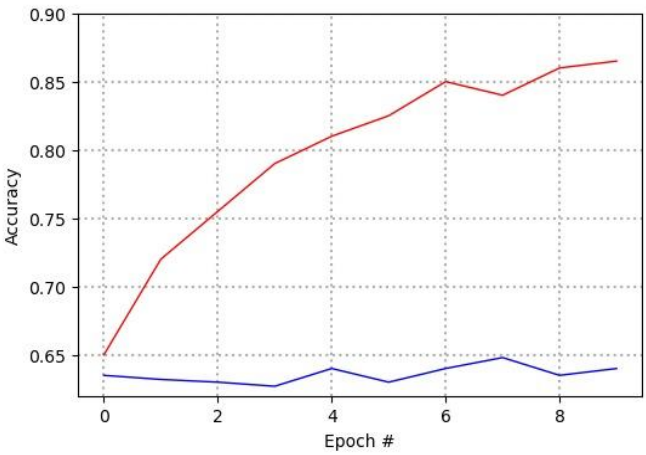

Figure 12. Training and validation of the proposed model

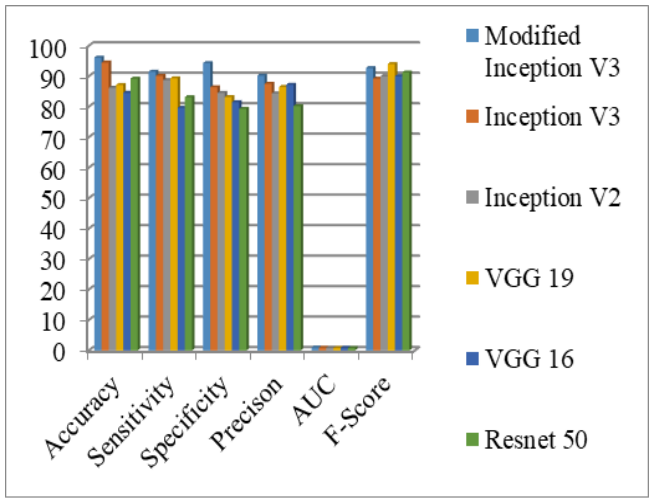

Figure 13. Performance comparison of proposed vs existing methods

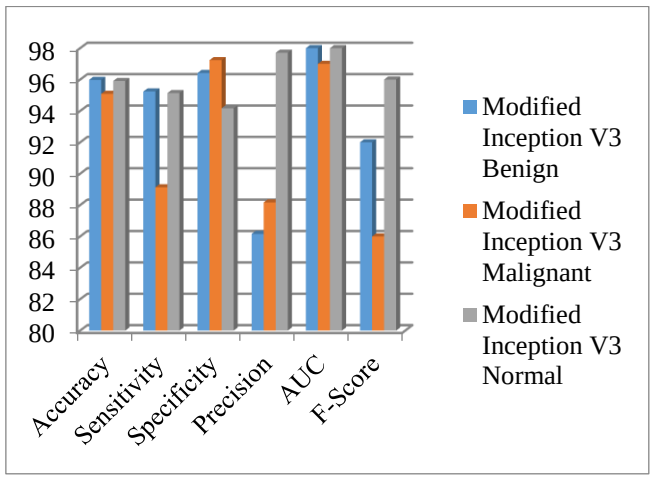

Figure 14. Performance comparison of proposed modified Inception v3 classifier

Table 5. Performance of proposed modified Inception v3 classifier

Modified Inceptionv3	ACC	SN	SP	PR	AUC	FS
Benign	95.98	95.24	96.42	86.16	98	92
Malignant	95.09	89.13	97.24	88.17	97	86
Normal	95.91	95.14	94.17	97.71	98	96

The results of the classifier's performance are shown in Table 4. The Modified Inception-V3 had the highest accuracy performance, while the Inception v3 scored second in accuracy, sensitivity, and specificity with 96.12%, 91.5%, and 94.3%, respectively. Figure 13 illustrates the Comparison among the proposed and existing methods.

Table 5 shows that the modified Inception v3 model outperforms other current models in classifying benign, malignant, and normal cases. Figure 14 illustrates the performance of the proposed Modified Inception v3 classifier.

7. CONCULSION

The accuracy of classifying mass lesions in the dataset was improved with the use of freezing and fine-tuning approaches.

The new model exhibited higher performance in comparison to four prior models in terms of accuracy, sensitivity, specificity, precision, area under the curve, and the F-score. Integrating the CNN via TL in the screening process leads to a significant improvement compared to previous methods. The findings indicated an accuracy of 96.12%, sensitivity of 91.5%, specificity of 94.3%, precision of 90.2%, F-score of 92.7%, and an AUC of 0.99. These findings surpass the other approaches listed.

The suggested approach may be applied in the future to diagnose other various cancer-related work. This work can also be implemented with real time patient detail to acquire more relevant accuracy of tumor prediction.

REFERENCES

[1] Lowry, K.P., Trentham-Dietz, A., Schechter, C.B., Alagoz, O., Barlow, W.E., Burnside, E.S., Stout, N.K. (2020). Long-Term outcomes and cost-effectiveness of breast cancer screening with digital breast tomosynthesis in the United States. JNCI: Journal of the National Cancer Institute, 112(6): 582-589. https://doi.org/10.1093/jnci/djz184

[2] George, S.A. (2000). Barriers to breast cancer screening: An integrative review. Health Care for Women International, 21(1): 53-65. https://doi:10.1080/073993300245401

[3] Viale, P.H. (2020). The American cancer Society's facts & figures: 2020 edition. Journal of The Advanced Practitioner in Oncology, 11(2): 135. https://doi:10.6004/jadpro.2020.11.2.1

[4] Zhou, J., Luo, L.Y., Dou, Q., Chen, H., Chen, C., Li, G.J., Jiang, Z.F., Heng, P.A. (2019). Weakly supervised 3D deep learning for breast cancer classification and localization of the lesions in MR images. Journal of Magnetic Resonance Imaging, 50(4): 1144-1151. https://doi.org/10.1002/jmri.26721

[5] Soomro, B.A., Lakhan, G.R., Mangi, S., Shah, N. (2020). Predicting entrepreneurial intention among business students of public sector universities of Pakistan: An application of the entrepreneurial event model. World Journal of Entrepreneurship, Management and Sustainable Development, 16(3): 219-230. https://doi.org/10.1108/WJEMSD-11-2019-0092

[6] Ting, F.F., Tan, Y.J., Sim, K.S. (2019). Convolutional neural network improvement for breast cancer classification. Expert Systems with Applications, 120: 103-115. https://doi.org/10.1016/j.eswa.2018.11.008

[7] Togacar, M., Özkurt, K.B., Ergen, B., Cömert, Z. (2020). BreastNet: A novel convolutional neural network model through histopathological images for the diagnosis of breast cancer. Physica A: Statistical Mechanics and its Applications, 545: 123592. https://doi:10.1016/j.physa.2019.123592

[8] Abbas, Q. (2016). DeepCAD: A computer-aided diagnosis system for mammographic masses using deep invariant features. Computers, 5(4): 28. https://doi.org/10.3390/computers5040028

[9] Sha, Z., Hu, L., Rouyendegh, B.D. (2020). Deep learning and optimization algorithms for automatic breast cancer detection. International Journal of Imaging Systems and Technology, 30(2): 495-506. https://doi.org/10.1002/ima.22400

[10] Lotter, W., Diab, A.R., Haslam, B., Kim, J.G., Grisot, G., Wu, E., Wu, K., Onieva, J.O., Boyer, Y., Boxerman, J.L., Wang, M., Bandler, M., Vijayaraghavan, G.R., Gregory Sorensen, A. (2021). Robust breast cancer detection in mammography and digital breast tomosynthesis using an annotation-efficient deep learning approach. Nature Medicine, 27(2): 244-249. https://doi.org/10.1038/s41591-020-01174-9

[11] Cao, H., Bernard, S., Heutte, L., Sabourin, R. (2018). Improve the performance of transfer learning without fine-tuning using dissimilarity-based multi-view learning for breast cancer histology images. In Image Analysis and Recognition: 15th International Conference, ICIAR 2018, Póvoa de Varzim, Portugal, Proceedings. Springer International Publishing. Springer, Cham, 15: 779-787. https://doi.org/10.1007/978-3-319-93000-8_88

[12] Deniz, E., Şengür, A., Kadiroğlu, Z., Guo, Y., Bajaj, V., Budak, Ü. (2018). Transfer learning based histopathologic image classification for breast cancer detection. Health Information Science and Systems, 6: 1-7. https://doi.org/10.1007/s13755-018-0057-x

[13] Celik, Y., Talo, M., Yildirim, O., Karabatak, M., Acharya, U.R. (2020). Automated invasive ductal carcinoma detection based using deep transfer learning with whole-slide images. Pattern Recognition Letters, 133: 232-239. https://doi.org/10.1016/j.patrec.2020.03.011

[14] Zhu, W., Ma, C., Zhao, X., Wang, M., Heidari, A.A., Chen, H., Li, C. (2020). Evaluation of sino foreign cooperative education project using orthogonal sine cosine optimized kernel extreme learning machine. IEEE Access, 8: 61107-61123. https://doi.org/10.1109/ACCESS.2020.2981968

[15] Lin, A., Wu, Q., Heidari, A.A., Xu, Y., Chen, H., Geng, W., Li, C. (2019). Predicting intentions of students for master programs using a chaos-induced sine cosine-based fuzzy K-nearest neighbor classifier. IEEE Access, 7: 67235-67248. https://doi.org/10.1109/ACCESS.2019.2918026

[16] Saber, A., Sakr, M., Abo-Seida, O.M., Keshk, A., Chen, H. (2021). A novel deep-learning model for automatic detection and classification of breast cancer using the transfer-learning technique. IEEE Access, 9: 71194-71209. https://doi.org/10.1109/ACCESS.2021.3079204

[17] Zhang, Y., Liu, R., Heidari, A.A., Wang, X., Chen, Y., Wang, M., Chen, H. (2021). Towards augmented kernel extreme learning models for bankruptcy prediction: algorithmic behavior and comprehensive analysis. Neurocomputing, 430: 185-212. https://doi.org/10.1016/j.neucom.2020.10.038

[18] Wei, Y., Ni, N., Liu, D., Chen, H., Wang, M., Li, Q., Ye, H. (2017). An improved grey wolf optimization strategy enhanced SVM and its application in predicting the second major. Mathematical Problems in Engineering, 2017(1): 9316713. https://doi.org/10.1155/2017/9316713

[19] Yu, C., Chen, M., Cheng, K., Zhao, X., Ma, C., Kuang, F., Chen, H. (2022). SGOA: Annealing-behaved grasshopper optimizer for global tasks. Engineering with Computers, 38(Suppl 5): 3761-3788. https://doi.org/10.1007/s00366-020-01234-1

[20] Cai, Z., Gu, J., Luo, J., Zhang, Q., Chen, H., Pan, Z., Li, Y., Li, C. (2019). Evolving an optimal kernel extreme learning machine by using an enhanced grey wolf

optimization strategy. Expert Systems with Applications, 138: 112814. https://doi.org/10.1016/j.eswa.2019.07.031

[21] Xu, Y., Chen, H., Heidari, A.A., Luo, J., Zhang, Q., Zhao, X., Li, C. (2019). An efficient chaotic mutative moth-flame-inspired optimizer for global optimization tasks. Expert Systems with Applications, 129: 135-155. https://doi.org/10.1016/j.eswa.2019.03.043

NOMENCLATURE

AUC	Area under the curve
ACC	Accuracy
FS	F-Score
GAP	Global average pooling
PR	Precision
SN	Sensitivity
SP	Specificity
TL	Transfer learning